Journal of the Korean Magnetic Resonance Society **2021**, *25*, 1-7
DOI http://dx.doi.org/10.6564/JKMRS.2021.25.1.001

Theoretical and practical features of *J*-scaled distortion-free HSQC

Jin Wook Cha[1,*] and Sunghyouk Park[2]

[1]Natural Product Informatics Research Center, KIST Gangneung Institute of Natural Products, Gangneung 25451, Republic of Korea
[2]Natural Product Research Institute, College of Pharmacy, Seoul National University, 1 Gwanak-ro, Gwanak-gu, Seoul 08826, Republic of Korea

Received Mar 19, 2021; Revised Mar 19, 2021; Accepted Mar 19, 2021

Abstract Employing of ^{13}C stable-isotopes in NMR metabolomics can give unique splitting patterns and coupling constants information originated from ^{13}C-^{13}C coupling interaction that provide an important structural information regarding the cellular metabolic process. But it has been known that an undesirable signal distortion in 2D heteronuclear correlation study, due to ^{13}C-^{13}C interaction, hampers an analysis of the coupling information. Recently, we proposed *J*-scaled distortion-free heteronuclear single-quantum coherence (HSQC) sequence which provides a distortion-free ^{13}C-^{13}C coupling information with a selective resolution enhancement of J_{CC} splitting. In this paper, we dicuss theoretical aspect and practical feature of *J*-scaled HSQC pulse sequence. The conceptual explanation of orgin of the signal distortion by ^{13}C-^{13}C coupling interaction and design of *J*-scaled HSQC through exemplified results are provided in brief.

Keywords ^{13}C-^{13}C coupling, ^{13}C-isotope, HSQC, *J*-scaling, NMR spectroscopy

Introduction

Recent development of high-resolution NMR spectrometers has enabled an obtaining of high-resolution signal in both direct and indirect domains in many *n*D NMR experiments.[1] Nevertheless, for nuclei with a wider range of chemical shift, such as ^{13}C, it is still challenge to acquire signals of resolution levels of several Hz in the indirect domain. On the other hands, for the cellular metabolic analysis based on NMR spectroscopy ^{13}C stable-isotope labeled compounds were widely employed to address low sensitivity problems on account of the low natural abundance and low gyromagnetic ratio of ^{13}C nucleus.[2] Together with the obtained high-sensitivity ^{13}C NMR signal, a specific J_{CC}-coupling pattern due to ^{13}C-^{13}C coupling interaction has been also exploited as a metabolic tracer in NMR metabolomics.[3] But, for the *J*-coupling analysis in HSQC, it is hard to extract coupling information such as splitting pattern or exact coupling constant due to the poor resolution and the signal distortion in the indirect domain.[4] Recently, we proposed *J*-scaled distortion-free HSQC sequence and reported its application for an analysis of metabolic mechanism of a drug with a cellular ^{13}C-isotopomer flux analysis.[5] Here, we will describe theoretical and practical aspects of the proposed sequence in brief.

Origin of the HSQC signal distortion by J_{CC}-coupling with ^{13}C-isotopes

The origins of signal distortion in the indirect domain of HSQC spectrum of the ^{13}C-isotope labeled compounds can be regarded as due to a polarization transfer of ^{13}C-^{13}C *J*-coupling modulated signal $S(t_1)$

* Address correspondence to: **Jin Wook Cha,** Natural Product Informatics Research Center, KIST Gangneung Institute of Natural Products, Gangneung 25451, Republic of Korea, Tel: 82-33-650-3511; E-mail: elmarit@kist.re.kr

during the t_1-evolution period. *J*-modulated signals consist of the combination of two trigonometric cosine and sine modulated *J*-coupling terms. In a more explicit expression, any constant delays, not the t_1-variable incremental delay, during the t_1-evolution period will give rise to the observable sine modulated *J*-coupling term (an origin of the dispersive anti-phase signal). For the non-^{13}C-isotope labeled compound, as the natural abundance of ^{13}C nucleus is low, their ^{13}C-^{13}C interaction can be neglected, as for whereas the uniformly ^{13}C-labeled compounds, which are frequently employed in cellular metabolomics study then the effect from ^{13}C-^{13}C interaction will be arisen.

Finite delays in t_1-evolution period by broadband inversion and gradient pulses

Modern NMR pulse sequence exploits adiabatic inversion[6] and gradient pulses.[7] Since an adiabatic spin inversion has many advantages, such as wide-range coverage, compare to a rectangular inversion pulse, it is not unusual an employing the adiabatic spin inversion for the nuclei which has a wide-range of chemical shift such as ^{13}C nucleus especially in a high-field NMR spectrometer.[8] Pulsed field gradient (PFG), in addition, is also an indispensable part for coherence transfer pathway selection and frequency discrimination in modern NMR experiments.[7] Each pulse, however, requires a finite delay of several milliseconds, which can be considered a constant delay that cannot be ignored on the NMR time scale.

Product operator analysis of the signal distortion in the indirect domain

As described above, the constant delay during the t_1-evolution period result in a phase distortion due to the survival of both cosine and sine J_{CC} coupling modulation terms during t_1. Assume that the product operator at a beginning of t_1-evolution period like as $-2\hat{S}_{1y}\hat{I}_z$ with a Hamiltonian $\hat{H}_0 = \Omega_{S_1}\hat{S}_{1z} + 2\pi J_{IS_1}\hat{I}_z\hat{S}_{1z} + 2\pi\sum_{k=2}^{L} J_{S_1S_k}\hat{S}_{1z}\hat{S}_{kz}$ where **I**- and **S**-spins denote ^{1}H and ^{13}C spin, respectively. Ω_{S_1} is the chemical shift of $\hat{S}_1$. J_{IS_1} and $J_{S_1S_k}$ are scalar coupling constants between **S**-spins in the subscripts. After incremental variable delay t_1 and constant delay Δ including a refocusing of hetero-nuclear coupling interaction the only observable operator has a form of

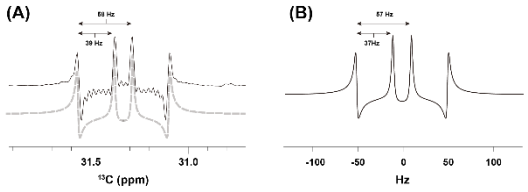

Figure 1. Comparison of actual HSQC using U-^{13}C-lactate (1 mM) and its simulated signal. (A) Overlay of 1D projection of actual HSQC spectrum (solid line) and simulated spectrum (dotted line). (B) The simulated spectrum. In simulated spectrum, ^{13}C-^{13}C coupling constants were set to 57 Hz and 36.5 Hz respectively. Delay Δ_t was set to 1.6 ms and R_2 relaxation constant was set to 0.3. For the Fourier transformation, $f_{\max}$ set to 4000 Hz and time-domain points were 150 complex points with the final 4096 complex points after zero-filling. For the apodization cosine-squared function was employed

$$2\hat{I}_y\hat{S}_{1z}\cos(\Omega_{S_1}t_1)\prod_{k=2}^{L}\cos\{\pi J_{S_1S_k}(t_1+\Delta)\} \qquad \textbf{(1)}$$

$$\cos(A+B) = \cos A\cos B - \sin A\sin B$$

where L is the number of coupled spin with S_1.

Thus, as the constant delay, Δ, increases by, a ratio of the undesirable dispersive anti-phase term (sine modulated term) is also increased together.

Acquiring a pure-phase inversion by a fast adiabatic inversion pulse pair

Since a constant delay in the t_1-evolution period is the origin of the signal distortion, a solution of these problem can be achieved through an introduction of fast adiabatic inversion pulses[9] and elimination of PFG in lieu of the conventional sequence. Thus, an introducing a fast broadband adiabatic inversion pulse can alleviate the generation of signal distortion. T-L. Hwang *et al.*[9] reported several fast adiabatic pulses including a tangential frequency sweeps which can accomplish a broadband inversion amount to tens of

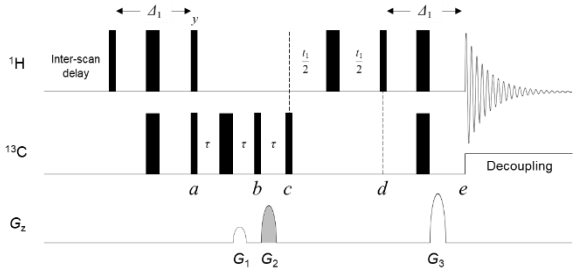

Figure 2. Exemplified pulse sequence for HSQC using gradient pulses with coherence selection step outside of the t_1-evolution period.

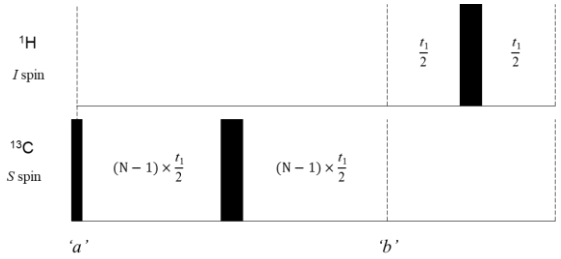

Figure 3. Proposed *N*-fold *J*-scaling module for two-dimensional HSQC.

kilohertz bandwidth using a practical B_1 strength. On the other hand, the single adiabatic inversion pulse cannot provide a desirable inversion for the transverse magnetization. Only magnetization collinear with a starting vector of the adiabatic pulse (*z*-magnetization) can follow B_1 field (adiabatic inversion).[8] There are two remedies to acquire a pure-phase refocusing of *xy*-magnetization, (1) composite adiabatic refocusing pulse[10] and (2) employing of adiabatic inversion pulse pair.[11] Because the composite adiabatic pulse has a four-fold duration compare to single adiabatic inversion pulse, it is not a proper choice. In contrast, the adiabatic inversion pulse pair only requires a half duration compare to composite adiabatic pulse. After applying the second identical transformation, each of transverse magnetization returns to their original states (pure phase inversion/refocusing) with the intensity of magnetization is attenuated according to the inversion efficiency.

Coherence selection by PFG outside of the t_1-evolution period

The coherence selection module (echo-anti echo frequency discrimination[12]) requires thousands of microseconds of length. Thereby, with ^{13}C-isotope labeled samples, for the distortion-free indirect domain signal the frequency discrimination by PFG in HSQC spectrum is no longer valid. STATES,[13] TPPI[14] or STATE-TPPI[15] acquisition methods are alternative methods can be used for the frequency discrimination without additional constant delays in many two-dimensional NMR experiments. But, contrary to PFG method, those methods give rise to t_1-noise which arisen from some instrumental imperfections regarding radio-frequency (RF) pulse. This t_1-noise, especially from strong signals, usually hampers analysis of weak signals in *in vivo* or cellular extract samples, generally exhibit low signal-to-noise ratio (SNR). To address this problem one can introduce PFG element instead of phase cycling by placing the PFG module before or after the t_1-evolution period. Figure 2 shows exemplified HSQC pulse sequence with coherence selection by PFG outside of the t_1-evolution period. Assume that, at an equilibrium state, the density operator has a form of $\hat{I}_z$. Then, at a point '*a*' the product operator became a form $-2\hat{S}_{1y}\hat{I}_z$ where, **I**- and **S**-spin denote ^{1}H and ^{13}C-spin, respectively. The Hamiltonian is $\hat{H}_0 = \Omega_{S_1}\hat{S}_{1z} + 2\pi J_{IS_1}\hat{I}_z\hat{S}_{1z} + 2\pi\sum_{k=2}^{L} J_{S_1S_k}\hat{S}_{1z}\hat{S}_{kz}$. Ω_{S_1} is the chemical shift of $\hat{S}_1$. J_{IS_1} and $J_{S_1S_k}$ are the scalar coupling constants between spins in the subscripts. ^{13}C-^{13}C coupling evolution during the rectangular pulse was ignored. Since the ratio of $G_1 : G_3 = 4 : 1$ and the observable form of operator is $\hat{I}_-$, the +1 coherence order of **S**-spin can only survive. Thus, before the acquisition, at a point '*e*', final observable operator has a form of

$$\frac{1}{4i}\hat{I}_- \exp(-i\Omega_{S1}t_1)\prod_{k=2}^{L}\cos(\pi J_{S_1S_k}t_1)\cos(2\pi J_{S_1S_k}\tau) \qquad \textbf{(2)}$$

where L is the number of coupled spin with S_1.

Thereby, N-type coherence selection by PFG outside the t_1-evolution period can give rise to a pure in-phase t_1-encoded signal with an enhanced SNR.

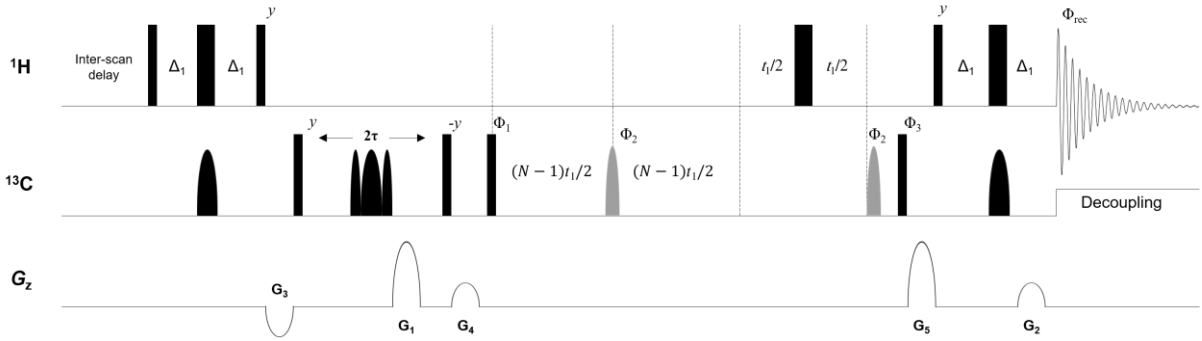

Figure 4. Pulse sequence of ^{13}C-^{13}C distortion-free *J*-scaled HSQC. Narrow and wide bars represent 90° and 180° hard pulses, respectively. Black semi-ellipse boxes indicate adiabatic inversion and refocusing pulses, respectively. Phase of Φ_1 and was shifted by 90° at every increment. $\boldsymbol{\Delta_1}$ was set to $1/4^1J_{CH}$. The phase cycling is as follows. $\Phi_1 = x, -x$; $\Phi 2 = -y, -y, y, y$; $\Phi_3 = -x, -x, x, x$ $\Phi_{rec} = x, -x, -x, x$. Gradient ratios: $G_1 : G_2 = 4 : 1$ and G_3, G_4 and G_5 are homospoil gradient pulses.

Implementation of *J*-scaling sequence into HSQC sequence

For the indirect domain the observation of fine structure and exact coupling constant values of multiplet have been limited due to poor spectral resolution. On the other hands, unlike direct acquisition period in t_2 where the time domain data is actually collected, the indirect detection scheme during the t_1-evolution period do not requires actual detection of signals by receiver of the spectrometer.[16] Thus, one can manipulate acquisition of the indirect detection scheme without the constraints of data acquisition scheme such as *J*-scaling.[17] In the following, first of all, detailed principles based on product operator formalism for *J*-scaling technique will be addressed and then the implementation of *J*-scaling sequence into actual HSQC pulse sequence will be described. Figure 3 exhibits a part of an exemplified *J*-scaling sequence for the HSQC sequence.

Suppose that a weakly coupled two spin system with a Hamiltonian in the rotating frame of reference $\widehat{H}_0 = \Omega_{S_1}\hat{S}_{1z} + 2\pi J_{S_1S_2}\hat{S}_{1z}\hat{S}_{2z}$ where **I**- and **S**-spin denote ^{1}H and ^{13}C-spin, respectively. Ω_{S_1} is the chemical shift of $\hat{S}_{1z}$ and $J_{S_1S_2}$ is the scalar coupling constant between weakly coupled spins $\mathbf{S}_1$ and $\mathbf{S}_2$.

Assume that at a point 'a' the density operator has a form of $2\hat{S}_{1y}\hat{I}_z$, after a free precession with an inversion pulse the density operator at 'b' is

$$-2\hat{S}_{1y}\hat{I}_z\cos\{(N-1)\pi J_{S_1S_2}t_1\} - \hat{S}_{1x}\sin\{(N-1)\pi J_{S_1S_2}t_1\} \quad \textbf{(3)}$$

A following pulse sequence gives

$$\begin{aligned}
&\cos\{(N-1)\pi J_{S_1S_2}t_1\}\cos(\Omega_{S_1}t_1)\{2\hat{S}_{1,y}\hat{I}_z\cos(\pi J_{S_1S_2}t_1) - \hat{S}_{1,x}\sin(\pi J_{S_1S_2}t_1)\}\\
&-\cos\{(N-1)\pi J_{S_1S_2}t_1\}\sin(\Omega_{S_1}t_1)\{2\hat{S}_{1,x}\hat{I}_z\cos(\pi J_{S_1S_2}t_1) + \hat{S}_{1,y}\sin(\pi J_{S_1S_2}t_1)\}\\
&-\sin\{(N-1)\pi J_{S_1S_2}t_1\}\cos(\Omega_{S_1}t_1)\{\hat{S}_{1,x}\cos(\pi J_{S_1S_2}t_1) + 2\hat{S}_{1,y}\hat{I}_z\sin(\pi J_{S_1S_2}t_1)\}\\
&-\sin\{(N-1)\pi J_{S_1S_2}t_1\}\sin(\Omega_{S_1}t_1)\{\hat{S}_{1,y}\cos(\pi J_{S_1S_2}t_1) - 2\hat{S}_{1,x}\hat{I}_z\sin(\pi J_{S_1S_2}t_1)\}
\end{aligned} \quad \textbf{(4)}$$

Using the trigonometric identity, it is simplified to

$$\begin{aligned}
&2\hat{S}_y\hat{I}_z\cos(\Omega_{S_1}t_1)\cos(N\pi J_{S_1S_2}t_1) - \hat{S}_x\cos(\Omega_{S_1}t_1)\sin(N\pi J_{S_1S_2}t_1)\\
&-2\hat{S}_x\hat{I}_z\cos(\Omega_{S_1}t_1)\cos(N\pi J_{S_1S_2}t_1) - \hat{S}_y\cos(\Omega_{S_1}t_1)\sin(N\pi J_{S_1S_2}t_1)
\end{aligned} \quad \textbf{(5)}$$

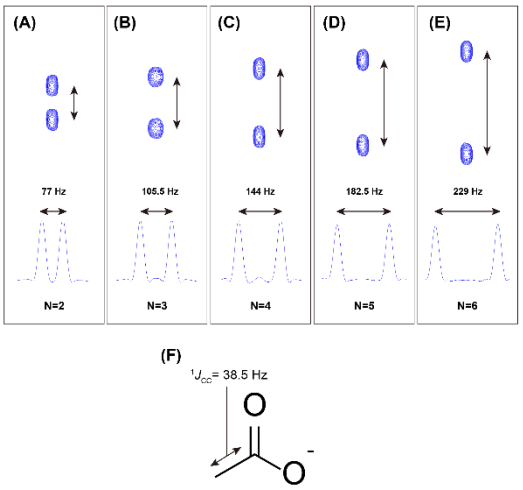

Figure 5. Comparison of scale-up of the *J*-coupling constant with difference scaling factor '*N*'. (A-E) The doublet signals of U-^{13}C acetate HSQC spectrum produced according to each scaling factor '*N*'. The bottom 1D signals are F_1 projection spectrum. (F) Structure of acetate and its $^{\mathbf{1}}\boldsymbol{J}_{\mathbf{CC}}$ coupling constants.

After an applying instantaneous $\pi/2(\hat{I}_x + \hat{S}_x)$ pulse at a point '*c*' the only observable **I**-spin operator is

$$-2\hat{S}_{1,z}\hat{I}_y \cos(\Omega_{S_1} t_1) \cos(\pi N J_{S_1 S_2} t_1) \qquad \textbf{(1)}$$

Based on result from Eq. **(6)**, a signal in t_1 of *N*-fold *J*-scaled HSQC with PFG outside t_1-evolution period can be expressed as

$$S(t_1) \propto \exp(-i\Omega_{S_1} t_1) \times \prod_{k=2}^{L} \cos\{\pi N J_{S_1 S_k}(t_1 + \Delta)\} \cos(2\pi J_{S_1 S_k} \tau) \qquad \textbf{(7)}$$

where Δ is the total constant delay in t_1-period, 2τ is the delay of PFG module outside of t_1-period and *L* is the number of coupled spin with S_1.

As a result, we can get the *N*-fold scaled ^{13}C-^{13}C scalar coupling interaction along the variable t_1 while its (**S**-spin; ^{13}C) chemical shift evolution is retained.

J-scaled distortion-free HSQC pulse sequence

Based on thus-obtained theoretical considerations, we have proposed the *J*-scaled distortion-free HSQC -

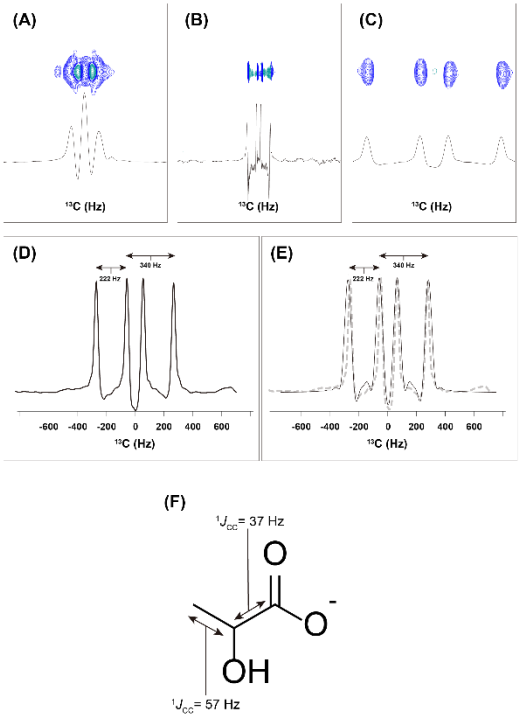

Figure 6. Comparison of HSQC signal of alpha carbon of U-^{13}C lactate. (A) Conventional HSQC signal (TD:300; uniform sampling). (B) Conventional HSQC signal (TD:3000; NUS 10% sampling density was used). (C) *J*-scaled HSQC signal (TD: 300, scaling factor: 6) (D) Enlarged of (C). (E) Simulated signal (solid line); Dotted line indicates signal of (D). (F) Structure of U-^{13}C lactate and its $^{\mathbf{1}}\boldsymbol{J}_{\mathbf{CC}}$-coupling constants.

experiment which provides high-resolution *J*-modulated pure absorptive signals in the indirect domain. Figure 4 shows a schematic pulse sequence of the proposed sequence and comparison of scale-up of the *J*-coupling constant by changing a scaling factor '*N*'. In figure 5, a coupling constant of doublet of U-^{13}C acetate methyl carbon signals were increased proportionally according to scaling factor. Finally, the HSQC signals acquired from the proposed pulse sequence (Figure 6) were compared with those produced by the conventional HSQC pulse sequence. To this end, using the U-^{13}C-lactate, conventional HSQC signals with the same t_1-time-domain point (TD: 300) and 3000 t_1-time-domain points were obtained and compared with the proposed *J*-scaled

HSQC signals (scaling factor = 6). In the case of conventional HSQC, the intact doublet of doublet signal at *alpha* carbon of U-^{13}C lactate did not appear due to poor resolution of the indirect domain (Figure 6A) and signal distortion (Figures 6A nd 6B). On the other hand, in the case of *J*-scaled HSQC signal (Figure 6C), despite the same sampling point value (TD: 300), the correct doublet of doublet signal could be confirmed due to the six-fold increased ^{13}C-^{13}C interaction effect, and signal distortion caused by anti-phase also rarely appeared. Of note, the simulated *J*-scaled HSQC signal according to the results derived from Eq. **(7)** also showed almost the same form as the actual signal (Figure 6D and 6E).

Practical considerations for *J*-scaled HSQC

For the choice of optimal *J*-scaling factor, in the proposed pulse sequence, the apparent size of the J_{CC} coupling constant in the indirect domain increases with the increase in the scaling factor, but the final signal resolution of the indirect domain of acquired two-dimensional spectrum is also affected by t_1-time-domain (TD) points, spectral width used. Therefore, the value of the optimal scaling factor depends on the several experiment parameters, and can be changed according to the isopotomer to be analyzed. Plus, note that an unconditional increase of the scaling factor can cause unintended signal separation and loss of signal sensitivity by J_{CC}-coupling of two or more bonds and increase the chance of overlapping with adjacent signals by the expanded signal splitting. The preservation of equivalent pathway (PEP)[18] in HSQC sequence can give a sensitivity enhancement ($\sqrt{2}$) by taking all two orthogonal magnetization parts where one part is generally discarded. Whereas the indirect domain signal of *J*-scaled HSQC signals at a uniformly ^{13}C-labeled CH$_n$ proton spin has a form of

$$S(t_1) \propto \sqrt{2}\cos(\Omega_{S_1} t_1)\cos^{n-1}(\pi J_{IS_1}\Delta_2) \times \prod_{k=2}^{L}\cos(\pi J_{S_1S_k}\Delta_2)\cos(2\pi J_{S_1S_k}\tau) \times \cos\{N\pi J_{S_1S_k}(t_1+\Delta)\} \quad \textbf{(8)}$$

where J_{IS_1} is the one-bond ^{1}H-^{13}C coupling constant , Δ_2 is the delay of the first reversed INEPT sequence in PEP module and L is the number of coupled spin with S_1. Since the PEP sensitivity factor, $\sqrt{2}\cos^{n-1}(\pi J_{IS}\Delta_2)\prod_{k=2}^{L}\cos(\pi J_{S_1S_k}\Delta_2)$ can be varied depends on an environment of functional groups in a molecule, PEP in *J*-scaled HSQC not always give a desirable sensitivity enhancement.

Conclusions

In this paper, theoretical explanations and practical considerations of the recently proposed experiment, *J*-scaled distortion-free HSQC sequence, were described briefly. *J*-scaled HSQC may be widely applied in metabolite analysis studies in which the concentration of a sample is low or a ^{13}C isotope-labeled compound is frequently used for analysis of a specific metabolic pathway. Through this paper, we hope an increasing interest of our proposed experiment, also look forward future improvement of technical aspect and expanding of application in more various fields.

Acknowledgements

This work was supported by the Korea Institute of Science & Technology—Research Program (2Z06482).

References

1. E. Moser, E. Laistler, F. Schmitt and G. Kontaxis, *Front. Phys.* **5** (2017)
2. R. Gruetter, G. Adriany, I. Y. Choi, P. G. Henry, H. Lei and G. Oz, *NMR Biomed.* **16**, 313 (2003)

3. S. Lee, H. Wen, Y. J. An, J. W. Cha, Y. J. Ko, S. G. Hyberts and S. Park, *Anal. Chem.* **89**, 1078 (2017)
4. U. Singh, S. Bhattacharya and B. Baishya, *J. Magn. Reson.* **311** (2020)
5. J. W. Cha, X. Jin, S. Jo, Y. J. An and S. Park, *Chem. Sci.*, DOI: 10.1039/d0sc06480g (2021)
6. E. Kupce and R. Freeman, *J. Magn. Reson., Ser A* **117**, 246 (1995)
7. J. Keeler, R. T. Clowes, A. L. Davis and E. D. Laue, *Methods Enzymol.* **239**, 145 (1994)
8. R. A. DeGraaf and K. Nicolay, *Concepts Magn. Reson.* **9**, 247 (1997)
9. T. L. Hwang, P. C. M. van Zijl and M. Garwood, *J. Magn. Reson.* **133**, 200 (1998)
10. T. L. Hwang, P. C. M. van Zijl and M. Garwood, *J. Magn. Reson.* **124**, 250 (1997)
11. T. L. Hwang and A. J. Shaka, *J. Magn. Reson., Ser A* **112**, 275 (1995)
12. J. Keeler and D. Neuhaus, *J. Magn. Reson.* **63**, 454 (1985)
13. D. J. States, R. A. Haberkorn and D. J. Ruben, *J. Magn. Reson.* **48**, 286 (1982)
14. D. Marion and K. Wuthrich, *Biochem. Biophys. Res. Commun.* **113**, 967 (1983)
15. D. Marion, M. Ikura, R. Tschudin and A. Bax, *J. Magn. Reson.* **85**, 393 (1989)
16. R. V. Hosur, *Prog. Nucl. Magn. Reson. Spectrosc.* **22**, 1 (1990)
17. W. Willker, U. Flogel and D. Leibfritz, *J. Magn. Reson.* **125**, 216 (1997)
18. A. G. Palmer, J. Cavanagh, P. E. Wright and M. Rance, *J. Magn. Reson.* **93**, 151 (1991)